International Journal of Systems Science
Vol. 42, No. 9, September 2011, 1473–1489

Taylor & Francis
Taylor & Francis Group

Distributed modal identification using restricted auto regressive models

Shamim N. Pakzad[a]*, Guilherme V. Rocha[b] and Bin Yu[c]

[a]*Department of Civil and Environmental Engineering, Lehigh University, Bethlehem, USA;* [b]*Department of Statistics, Indiana University, Bloomington, USA;* [c]*Department of Statistics, University of California, Berkeley, USA*

(*Received 28 September 2010; final version received 9 January 2011*)

Advances in Wireless Sensor Networks (WSN) technology have provided promising possibilities in detecting a change in the state of a structure through monitoring its features estimated using sensor data. The natural vibration properties of the structure are a set of features commonly used for this purpose and are often estimated using a multivariate autoregressive model (AR model) for the measured structure's response to ambient vibrations. Fitting a multivariate AR model to the observed acceleration requires the computation of the lagged covariance between the measurements in all nodes. The resulting volume of data transmission causes significant latency due to the low data bandwidth of WSNs in addition to having a high transmission energy cost. In this paper, a set of restrictions to the estimation of the AR model is introduced. Such restrictions significantly reduce the volume of data flowing through the WSN thus reducing the latency in obtaining modal parameters and extending the battery lifetime of the WSN. A physical motivation is given for the restrictions based on a linear model for a multi-degree of freedom vibrating system. Stabilisation diagrams are compared for the restricted and full AR models fitted using data simulated from linear structures and real data collected from a WSN deployed on the Golden Gate Bridge (GGB). These stabilisation diagrams show that the estimated modes using the restricted AR models are of comparable quality to that of the full AR model while substantially reducing the volume of transmitted data.

Keywords: modal identification; distributed processing; wireless sensor networks; bridge monitoring; restricted models

1. Introduction

With the advances in Wireless Sensor Network (WSN) technology both in terms of hardware design and software architecture, and their increasingly widespread application in structural engineering, novel data processing techniques are viewed as essential tools to enhance the performance of the integrated systems (Kim et al. 2007). In wired sensor networks, the data collection paradigm assumes ample availability of power and communication bandwidth in the entire network. With this assumption, there is little cost to transfer each and every measurement to a central processing location, where data processing operations, including filtering and digitisation, are performed. The latency in collecting and processing the data at the central processing location is minimal due to the high data transmission bandwidth capacity in a wired network.

In contrast to wired sensor networks, WSNs can operate at lower installation and maintenance cost, while allowing data to be collected at higher spatial and temporal resolution. To fully reap the benefits of WSN, energy use must be carefully budgeted. That, in turn, requires that data transmission be kept to a minimum, since data transmission is the most energy expensive task in a WSN. Unlike wired sensor networks, a node in a WSN has considerable processing power that could be exploited to save power. In-network processing can save energy, since communicating one bit of data is about 10,000 times more energy intensive than performing an arithmetic operation on that same bit (Glaser and Tolman 2008). This is evident, for example, by comparing the power requirement of a common CC2420 transceiver which consumes $240\,\mu W - sec$ for a single hop transmission of 1 kB data, versus $25\,nW - sec$ power consumed for performing a flop on 1 kB data by PXA27x Processor used in Imote2 devices. In addition to the energy cost, latency in analysis is a compelling reason for keeping data transmission to a minimum. Due to the limited communication bandwidth in a WSN, transmitting large volumes of data from the sensors to a central location can take a prohibitively long time.

Natural vibration properties of the structure have been the focus of many studies in structural health monitoring (SHM) and provide a great insight into the condition of the structure (Abdel-Ghaffar and Scanlan

*Corresponding author. Email: pakzad@lehigh.edu

ISSN 0020–7721 print/ISSN 1464–5319 online

DOI: 10.1080/00207721.2011.563875
http://www.informaworld.com

1985a,b; Doebling, Farrar, and Prime 1998; Chang, Chang, and Zhang 2001; Cunha, Caetano, and Delgado 2001; Farrar 2001). The objective of modal identification process is to estimate the natural vibration properties of a structure, i.e. its natural frequencies, damping ratios and mode shapes, using the measured response of the system to ambient or forced excitations. Several methods exist for identifying the modal parameters of a structure, such as Eigen Realisation Algorithm (ERA), Multivariate Autoregressive Moving Average with Exogenous models (ARMAX), and Ibrahim Time Domain method (ITD) and Stochastic Subspace Identification technique (SSI); see Doebling et al. (1998) and Sohn, Farrar, Hemez, Czarnecki, Shunk, and Stinemates (2004) for a more complete list and further information. Olfati-Saber (2007) and Shen, Wang, and Hung (2010) present recent studies on the distributed state estimation of WSN. For linear systems, all of these modal identification methods rely either explicitly or implicitly on the space–time covariance of measured responses of the structure.

This article focuses on a popular modal identification method based on fitting a multivariate autoregressive model (AR model) to the measurements of the structure's response to ambient vibrations. The contribution of this article is to introduce a distributed form of multivariate AR models that are suited for wireless networks, resulting in a shorter delay in identification of modal properties of the monitored structure, with a lower communication power requirement. In the AR model, the observed response at time t is modelled as a linear relationship between the observed responses at times $t-1,\ t-2, \ldots, t-q$. The coefficients in this linear model capture the temporal and spatial covariances of the observed responses at different points in time and space. These autoregressive coefficients can be converted into estimates for the natural frequencies, damping ratios and mode shapes of the structure as detailed in Andersen (1997). In its original form, this strategy is ill-suited for use with WSNs: computing least squares estimates of the parameters of an AR model requires computation of the auto-covariance between lagged measurements in all nodes, as shown in Section 2.2. While this is not an issue in wired networks, in WSNs estimation of the complete covariance matrix is extremely costly both in terms of energy and latency as the covariance of data on nodes on opposite ends of the communication network must be computed.

A restricted form of the multivariate AR model is introduced in this article. The restrictions correspond to the assumption that the direct effect of a node on a distant node is negligible. In other words, nodes that are 'spatially' distant do not have a direct effect on each other. In terms of the AR model, this corresponds to simply setting some of the coefficients to zero. Indeed, the decision to focus on AR model-based identification method follows from this explicit relation between the model coefficients and distances in time and space. A physical motivation for the spatial restrictions is offered using a linear multi-degree of freedom model. The restrictions are shown to significantly reduce the volume of data transmitted over the WSN, thus extending the lifetime of the batteries and reducing the latency in obtaining the modal parameter estimates. The restrictions can be adjusted to control the volume of transmitted data, with the full AR model corresponding to the least restricted version of the restricted models. Data simulated from a linear vibrating system subjected to random excitations are used to contrast the modal parameters estimated using the restricted and full AR models. A comparison of the stabilisation diagrams for the full AR model and different restricted models reveals that it is possible to identify the modal properties of the structure while greatly reducing the volume of transmitted data.

The restricted AR modal parameter estimation algorithm is then applied to a data set from the deployment of a WSN on Golden Gate Bridge (GGB). This experiment, which was the largest deployment of WSNs on a civil infrastructure at the time it was deployed, included 64 sensing units (for a total of 320 sensors) on the main span and the south tower of the bridge, and produced 174 complete and partial data sets of ambient acceleration and temperature (Pakzad, Fenves, Kim, and Culler 2008; Pakzad and Fenves 2009; Pakzad 2010). A sample data set from sensor nodes on both sides of the main span is used to compare the modal properties from the restricted and full models. The stabilisation diagrams show that the modal properties estimated by the restricted AR model agree well with the results from the AR model at a fraction of the total data transmission volume.

The remainder of this article is organised as follows. Section 2 reviews one of the existing methods for estimating modal parameters based on AR models. Section 3 introduces the restricted AR model and discusses estimation of its parameters, its data trasmission savings and its physical motivation. Section 4 presents a comparison of the stabilisation diagrams resulting from using the full and restricted versions of the AR model. Through stabilisation diagrams, Section 5 presents a comparison of the full and restricted AR models when applied to data collected from GGB. Section 6 concludes with a short summary of the results and a discussion of possible extensions.

2. Multivariate AR models

Multivariate AR models are often used to model the dynamic behaviour of the response measured at different nodes of a vibrating structure. Such models are known to yield stable, reliable and accurate estimates of the dynamic properties of a structure (Pandit 1991; Peeters and Roeck 2001; Pakzad et al. 2008). The $AR(q)$ model of measured accelerations for estimating modal parameters is reviewed in this section.

2.1. *Formulation of the multivariate AR(q) model*

Let $s(t)$ denote a p-dimensional vector of the displacement of the structure from equilibrium at the positions of the p sensing units at time t. The dot notation is used to represent derivatives with respect to time: $\dot{s}(t)$ and $\ddot{s}(t)$ represent vectors of instantaneous speeds and accelerations, respectively. Acceleration measurements are made at discrete time steps with sampling period Δt. The vector of measured accelerations at time $k\Delta t$ is denoted by $\ddot{u}(k)$.

The q-th order Auto Regressive – $AR(q)$ – model for the acceleration response $\ddot{u}(k)$ is

$$\ddot{u}(k) = \sum_{j=1}^{q} L_j^{(q)} \ddot{u}(k-j) + v(k), \tag{1}$$

where

$$\ddot{u}(k) = \begin{bmatrix} \ddot{s}_1(k\Delta t) \\ \ddot{s}_2(k\Delta t) \\ \vdots \\ \ddot{s}_p(k\Delta t) \end{bmatrix}, \; L_j^{(q)} = \begin{bmatrix} \beta_{1,1,j} & \beta_{1,2,j} & \cdots & \beta_{1,p,j} \\ \beta_{2,1,j} & \beta_{2,2,j} & \cdots & \beta_{2,p,j} \\ \vdots & \vdots & \ddots & \vdots \\ \beta_{p,1,j} & \beta_{p,2,j} & \cdots & \beta_{p,p,j} \end{bmatrix},$$

$$v(k) = \begin{bmatrix} v_1(k\Delta t) \\ v_p(k\Delta t) \\ \vdots \\ v_p(k\Delta t) \end{bmatrix}.$$

In this equation, $L_j^{(q)}$ is the matrix of coefficients for lag j of the $AR(q)$ model and $v(k)$ is a vector of error terms due to random excitation on the structure and measurement errors. Note that the number of lags to use is part of the estimation problem. For modal estimation, stabilisation diagrams are used to select an adequate number of lags (see, for instance, Lembregts, Snoeys, and Leuridan 1992; Pandit 1991). Formally, the choice of the number of lags can be represented as restrictions on the model coefficients $\beta_{i_1,i_2,j} = 0$ for all $j > q$. Intuitively, these restrictions represent the idea that observations in the more distant past do not affect the current observed response directly. The restricted version of the AR model proposed in this article amounts to adding spatial restrictions to these temporal restrictions, as detailed in Section 3.1.

2.2. *Estimation of the AR(q) model parameters*

The parameters in the full $AR(q)$ models can be estimated by minimising the sum of squared residuals. The data matrices are defined as follows:

$$\ddot{V} = \begin{bmatrix} \ddot{u}(q)^T & \ddot{u}(q-1)^T & \cdots & \ddot{u}(1)^T \\ \ddot{u}(q+1)^T & \ddot{u}(q)^T & \cdots & \ddot{u}(2)^T \\ \ddot{u}(q+2)^T & \ddot{u}(q+1)^T & \cdots & \ddot{u}(3)^T \\ \vdots & \vdots & \ddots & \vdots \\ \ddot{u}(T-2)^T & \ddot{u}(T-3)^T & \cdots & \ddot{u}(T-q-1)^T \\ \ddot{u}(T-1)^T & \ddot{u}(T-2)^T & \cdots & \ddot{u}(T-q)^T \end{bmatrix}. \tag{2}$$

and

$$\ddot{W} = \begin{bmatrix} \ddot{u}(q+1)^T & \ddot{u}(q+2)^T & \ddot{u}(q+3)^T & \cdots & \ddot{u}(T-1)^T & \ddot{u}(T)^T \end{bmatrix}^T, \tag{3}$$

where the double dots represent acceleration measurements. $\ddot{V}$ is the data matrix of lagged measured accelerations and $\ddot{W}$ is the data matrix of current measured accelerations. The least squares estimate

$$\hat{L}^{(q)} = \begin{bmatrix} \left(\hat{L}_1^{(q)}\right)^T & \left(\hat{L}_2^{(q)}\right)^T & \cdots & \left(\hat{L}_q^{(q)}\right)^T \end{bmatrix}^T \in R^{pq \times p}$$

can be written as

$$\hat{L}^{(q)} = \underset{L \in R^{pq \times p}}{\arg\min} \left\{ \mathrm{tr}\left[\left(\ddot{W} - \ddot{V}L\right)^T \left(\ddot{W} - \ddot{V}L\right) \right] \right\}, \tag{4}$$

Let $L_{\bullet,i}^{(q)}$ and $\ddot{W}_{\bullet,i}$ denote the i-th columns of L and $\ddot{W}$ matrices respectively. It is then easy to show that

$$\mathrm{tr}\left[\left(\ddot{W} - \ddot{V}L\right)^T \left(\ddot{W} - \ddot{V}L\right) \right] = \sum_{i=1}^{p} \left(\ddot{W}_{\bullet,i}^T \ddot{W}_{\bullet,i} - 2\ddot{W}_{\bullet,i}^T \ddot{V} L_{\bullet,i} + L_{\bullet,i}^T \ddot{V}^T \ddot{V} L_{\bullet,i} \right).$$

Since each term of this sum involves only the optimisation parameters in $L_{\bullet,i}$, the optimisation problem can be split into p smaller problems and $\hat{L}_{\bullet,i}^{(q)}$ the i-th column of the $\hat{L}^{(q)}$ matrix is

$$\hat{L}_{\bullet,i}^{q} = \underset{L_{\bullet,i} \in R^{pq \times 1}}{\arg\min} \left[\ddot{W}_{\bullet,i}^T \ddot{W}_{\bullet,i} - 2\ddot{W}_{\bullet,i}^T \ddot{V} L_{\bullet,i} + L_{\bullet,i} \ddot{V}^T \ddot{V} L_{\bullet,i}^T \right]. \tag{5}$$

Equation (5) shows that in order to obtain an estimate of the coefficients $\beta_{i_1,i_2,j}$ for a fixed i_1 the following two summaries of the data are needed: the pq-dimensional row vector $\ddot{W}_{\bullet,i}^T \ddot{V}$ and the $pq \times pq$

matrix $\ddot{V}^T\ddot{V}$. In terms of the individual acceleration observations, these summaries can be written as

$$\ddot{W}_{\cdot,i}^T\ddot{V} = \sum_{k=q+1}^{T} \ddot{u}_i(k)[\ddot{u}(k-1)^T \quad \ddot{u}(k-2) \quad \cdots \quad \ddot{u}(k-q)^T], \quad \text{and}$$

$$\ddot{V}^T\ddot{V} = \sum_{k=1}^{T-q} \begin{bmatrix} \ddot{u}(k+q-1)\ddot{u}(k+q-1)^T & \ddot{u}(k+q-1)\ddot{u}(k+q-2)^T & \cdots & \ddot{u}(k+q-1)\ddot{u}(k)^T \\ \ddot{u}(k+q-2)\ddot{u}(k+q-1)^T & \ddot{u}(k+q-2)\ddot{u}(k+q-2)^T & \cdots & \ddot{u}(k+q-2)\ddot{u}(k)^T \\ \vdots & \vdots & \ddots & \vdots \\ \ddot{u}(k)\ddot{u}(k+q-1)^T & \ddot{u}(k)\ddot{u}(k+q-2)^T & \cdots & \ddot{u}(k)\ddot{u}(k)^T \end{bmatrix}.$$

Since all columns of $\hat{L}^{(q)}$ are needed, it is clear that the summaries of the data above are equivalent to estimating all pairwise empirical covariances

$$\hat{\rho}_{i_1,i_2,j} = \frac{1}{T}\sum_{k=q+1}^{T} \ddot{u}_{i_1}(k-1)\ddot{u}_{i_2}(k),$$
$$\text{for all } i_1, i_2 \in \{1,\ldots,p\} \quad \text{and} \quad j = 0,\ldots,q.$$

In summary, least squares estimates for the AR coefficient matrices can be computed in terms of p separate problems. While this allows for some distribution of the processing over the network, each node still needs to receive data from all other nodes to solve its share of the estimation problem. As will be shown in Section 3.2, the restricted version of the AR model can be estimated based on a smaller subset of these covariances.

2.3. *Modal parameters from AR(q) model parameters*

To obtain the modal parameters of the structure from the parameters of the AR model in Equation (1), the AR model is converted to state–space form

$$\ddot{U}_q(k) = R_q\ddot{U}_q(k-1) + Y(k), \tag{6}$$

with

$$\ddot{U}_q(k) = \begin{bmatrix} \ddot{u}(k)^T & \ddot{u}(k-1)^T & \cdots & \ddot{u}(k-q+1)^T \end{bmatrix},$$

a pq-dimensional vector,

$$R_q = \begin{bmatrix} L_1^{(q)} & L_2^{(q)} & \cdots & L_{q-1}^{(q)} & L_q^{(q)} \\ I_p & 0 & \cdots & 0 & 0 \\ 0 & I_p & \cdots & 0 & 0 \\ \vdots & \vdots & \ddots & \vdots & \vdots \\ 0 & 0 & \cdots & I_p & 0 \end{bmatrix},$$

a $pq \times pq$ matrix and

$$Y(k) = \begin{bmatrix} v(k)^T & 0_{1\times p} & \cdots & 0_{1\times p} \end{bmatrix},$$

a pq-dimensional vector.

The companion matrix R_q contains information about the dynamic behaviour of the vibrating structure. In particular, it contains information about the frequency and speed of decay of the vibrations, resulting from an impulse applied to the structure. The modal parameters summarise such information and are then obtained from the spectral decomposition of the system matrix $R_q = \Psi_q\Lambda_q\Psi_q^*$, where Λ_q is a complex valued pq-dimensional diagonal matrix of eigenvalues $\lambda_i, j = 1,\ldots,pq$ and Ψ_q is a matrix containing the (complex) eigenvectors of R_q in its columns.

Following Andersen (1997), the Ψ_q matrix of eigenvectors has the form

$$\Psi_q = \begin{bmatrix} \Psi_1\lambda_1^{q-1} & \Psi_2\lambda_2^{q-1} & \cdots & \Psi_{pq-1}\lambda_{pq-1}^{q-1} & \Psi_{pq}\lambda_{pq}^{q-1} \\ \Psi_1\lambda_1^{q-2} & \Psi_2\lambda_2^{q-2} & \cdots & \Psi_{pq-1}\lambda_{pq-1}^{q-2} & \Psi_{pq}\lambda_{pq}^{q-2} \\ \vdots & \vdots & \ddots & \vdots & \vdots \\ \Psi_1\lambda_1^{1} & \Psi_2\lambda_2^{1} & \cdots & \Psi_{pq-1}\lambda_{pq-1}^{1} & \Psi_{pq}\lambda_{pq}^{1} \\ \Psi_1 & \Psi_2 & \cdots & \Psi_{pq-1} & \Psi_{pq} \end{bmatrix},$$

where each Ψ_j is a p-dimensional vector for $j = 1,\ldots,pq$. Only p of all Ψ_{pq} eigenvectors represent structural mode shapes. The remaining $p(q-1)$ vectors correspond to spurious computational modes. The frequency ω_j and damping ratios ς_j for each of the modes is extracted from the eigenvalues by

$$\omega_j = \frac{|\log(\lambda_j)|}{\Delta t}, \quad \text{and} \quad \varsigma_j = \frac{\mathrm{Re}(\log(\lambda_j))}{|\log(\lambda_j)|}.$$

Several criteria are used to separate the p physical modes from the $p(q-1)$ spurious computational modes. One of these criteria, for instance, is to require that the estimated damping ratio for a mode be below a certain threshold consistent with the expected damping ratio of the physical structure. In this article, stabilisation diagrams are also used to discard computational modes. A stabilisation diagram is a graphical presentation for the convergence of the model, as the model order is increased. The concept arises from the fact that spurious computational modes are generally not consistent, and appear or disappear as the model order changes. Convergence criteria for natural vibration frequencies, damping ratios and mode shapes are

chosen such that the spurious modes are rejected and do not appear in the stabilisation diagram. In the simulations and experiment presented in Sections 4 and 5, modes estimated by the $AR(q)$ model are considered stable if their natural frequency, damping ratio and mode shape collinearity change by less than 2%, 5% and 5% respectively from the modes found in the $AR(q-2)$ model. For more information about the application of stabilisation diagrams and alternative stability criteria, see Andersen (1997).

3. Restricted AR models

This section describes the main contribution of this article: a restricted version of the multivariate $AR(q)$ model which can be estimated with a reduced communication load on the WSN collecting the data. From a statistical standpoint, the restrictions can also result in improved estimates in large WSNs since they are based on physical properties of the modelled structure. Section 3.5 includes a physical motivation for the restrictions based on the physical model for a vibrating structure.

3.1. *Formulation of the restricted AR(w,q) model*

As previously mentioned, the $AR(q)$ model contains an implicit set of restrictions as it sets $\beta_{i_2,i_2,j}=0$ for all $j>q$. Such restrictions can be interpreted as an assumption that observations in the distant past should have no direct effect on present observations. The restrictions proposed in this article can be interpreted as the spatial counterpart of the temporal restrictions made by the AR: they correspond to an assumption that measurements in nodes that are far apart in space do not have a direct effect on each other, or that their effect is indirectly accounted for by the measurements at closer nodes.

One complication with introducing such restrictions is that, unlike time, different metrics can be used to represent the distance between two elements in space. To define a suitable notion of distance between acceleration measurements in the structure, a graph representing direct communication links between points in the structure is created. The distance $d(i_1,i_2)$ between nodes i_1 and i_2 is defined as the minimum number of hops needed to travel between the two nodes. A hop is defined here as the smallest wireless communication unit between a sensor node and the node adjacent to it. Just as the $AR(q)$ in time sets $\beta_{i_2,i_2,j}=0$ if $j>q$, the restriction $\beta_{i_2,i_2,j}=0$ if $d(i_1,i_2)>w$ is imposed for a certain threshold $w>0$. In Figure 1(i), this restriction is demonstrated in a structure with a linear topology, along with the corresponding connection graph and the hop-distance between nodes. The restricted-$AR(w,q)$ model is then represented by

$$\ddot{u}(k)=\sum_{j=1}^{\infty}L_j^{(q,w)}\ddot{u}(k-j)+v(k), \tag{7}$$

where for each matrix of coefficients $L_j^{(q,w)}$, the parameters $\beta_{i_2,i_2,j}=0$ whenever $d(i_1,i_2)>w$ or $j>q$. For a structure with linear topology as shown in Figure 1(i), these restrictions result in banded coefficient matrices. Setting $w=1$, for instance, leads to matrices of coefficients where the only possibly non-zero parameters are in a band of distance one from the diagonal.

As the notation $L_j^{(q,w)}$ suggests, the problem of selecting a proper bandwidth w is akin to that of selecting a proper number of lags q for the autoregressive model. In Sections 4 and 5, the effects of using different bandwidths w in the estimates of the modal parameters are illustrated, both in simulated and real data settings. Criteria for automatic selection of the width w will be the subject of future research.

3.2. *Estimating modal parameters using the restricted AR(w,q) model*

As is the case for the full $AR(q)$ model, the parameters of the restricted $AR(w,q)$ model can be estimated by the least squares method. However, unlike the full $AR(q)$ model, estimation of the restricted $AR(w,q)$ model only requires the lagged covariances of a subset of pairs of nodes. To estimate the coefficients of the restricted $AR(w,q)$ model, for each node i, define the neighbourhood $N_i=\{i_2 : d(i,i_2)\le w\}$, the neighbourhood size p_i and the data matrix

$$\ddot{V}_{N_i}=\begin{bmatrix}\ddot{u}_{N_i}(q)^T & \ddot{u}_{N_i}(q-1)^T & \cdots & \ddot{u}_{N_i}(1)^T\\ \ddot{u}_{N_i}(q+1)^T & \ddot{u}_{N_i}(q)^T & \cdots & \ddot{u}_{N_i}(2)^T\\ \ddot{u}_{N_i}(q+2)^T & \ddot{u}_{N_i}(q+1)^T & \cdots & \ddot{u}_{N_i}(3)^T\\ \vdots & \vdots & \ddots & \vdots\\ \ddot{u}_{N_i}(T-2)^T & \ddot{u}_{N_i}(T-3)^T & \cdots & \ddot{u}_{N_i}(T-q-1)^T\\ \ddot{u}_{N_i}(T-1)^T & \ddot{u}_{N_i}(T-2)^T & \cdots & \ddot{u}_{N_i}(T-q)^T\end{bmatrix},$$

a $(T-q)\times p_i q$ matrix, where $\ddot{u}_{N_i}(q)$ is a p_i dimensional vector of measured accelerations at time step k at the positions in the neighbourhood N_i. By imposing the restrictions $\beta_{i_2,i_2,j}=0$ when $d(i_1,i_2)>w$ to the least squares estimation problem, we get

$$\hat{L}_{\bullet,i}^{(q,w)}=\underset{L_{\bullet,j}\in p_i q\times 1}{\arg\min}\left[L_{\bullet,i}^T\cdot\left(\ddot{V}_{N_j}^T\ddot{V}_{N_i}\right)\cdot L_{\bullet,i}-2\cdot\left(\ddot{W}_{N_i}^T\ddot{V}_{N_i}\right)\cdot L_{\bullet,i}\right]. \tag{8}$$

Based on Equation (8), it is observed that only the sample auto-covariances for pairs (i_1,i_2) of nodes

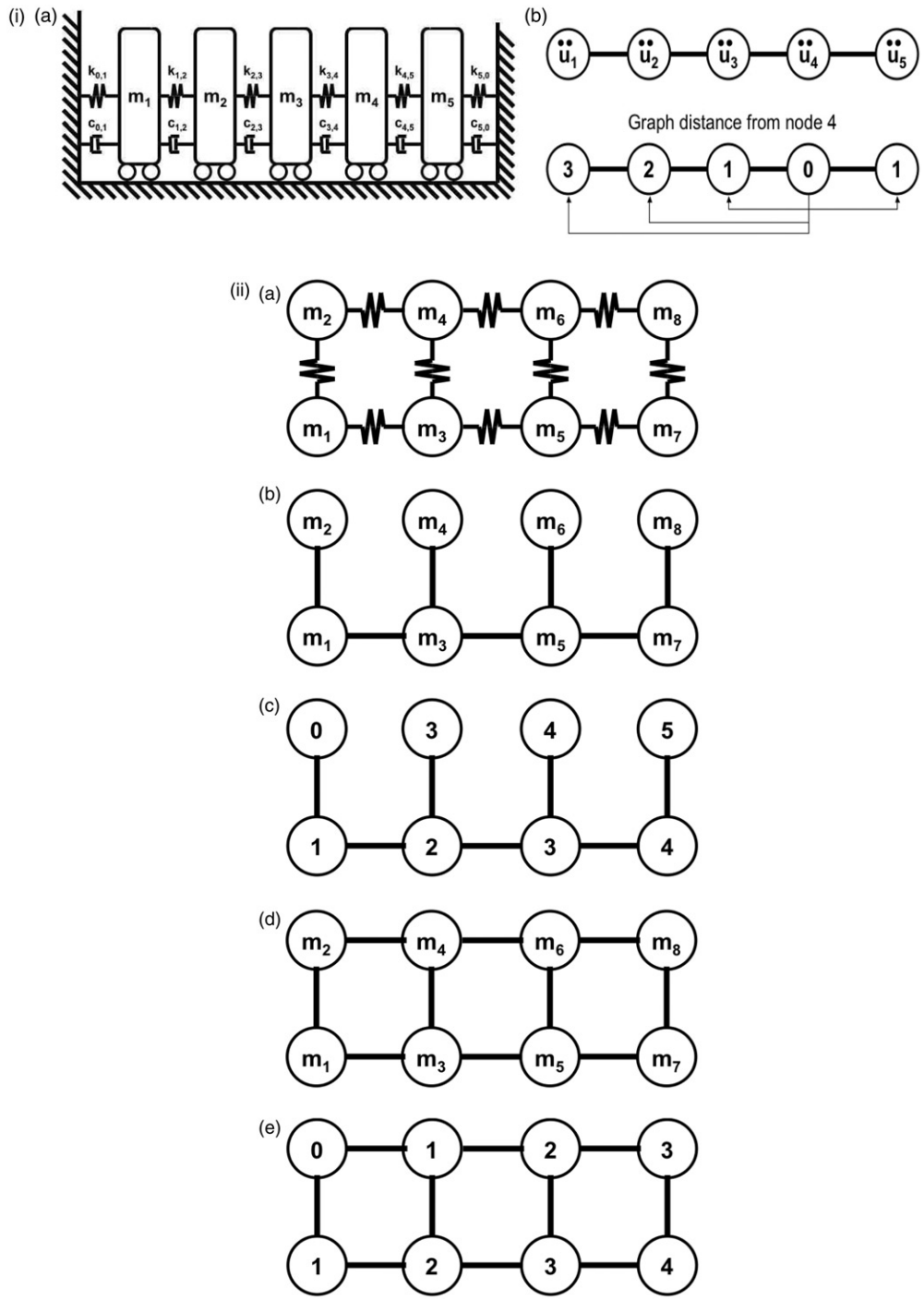

Figure 1. (i) Structure with linear topology. (a) Linear topology structure with five nodes and (b) Hop distance from node 4. Each node in the structure is only connected to its closest neighbours. (ii) Structure with different communication and physical topologies. (a) Physical topology; (b) Case 1 communication topology; (c) Hop distance from node 2 in Case 1; (d) Case 2 communication topology; and (e) Hop distance from node 2 in Case 2.

satisfying $d(i_1, i_2) \leq w$ must be computed. By selecting a suitable w, the number of summaries (covariances) needed to compute the estimates of the restricted-$AR(w,q)$ model can be substantially smaller than that required by the full $AR(q)$ model. The modal parameters are obtained from the parameters of the restricted-$AR(w,q)$ model in the same fashion described in Section 2.3.

3.3. *Communication load savings using restricted-AR(w,q)*

The estimation of the coefficients in the full AR process requires that each node compute its correlations with all other nodes up to lag q. For the restricted model, computing the coefficients associated with node i_1 only requires the correlations with the nodes i_2 such that $d(i_1, i_2) \leq w$. Suppose that each node transmits its data to all other nodes that need it to compute the estimates for its AR parameters. The transmission volume over the wireless network can be computed based on the number of sample-hops that is necessary to estimate the model. For a network with a linear topology the signal at each node must be transmitted to all other nodes in the network. The total transmission volume in this case is $\frac{np(p+1)}{2}$ with order $O(np^2)$, where p is the number of nodes in the network and n is the number of samples at each node. For the restricted model, each node has to communicate its data over a graph with diameter $2w$, with a transmission volume of

$$\begin{aligned} &n[2w(p-2w)+2[(2w-1)+(2w-2)+\cdots+(2w-w)]] \\ &\quad = n[2wp-w^2-w], \end{aligned} \tag{9}$$

or $O(nwp)$. This corresponds to an efficiency ratio of $O(\frac{w}{p})$, which could be a significant saving in communication load of the network. In Sections 4 and 5, simulated and WSN data sets are used to show that good estimates of the modal parameters can be obtained with $\frac{w}{p}$ as low as $\frac{1}{7}$.

3.4. *Restrictions to AR model and statistical regularisation*

In addition to reducing the communication load in the network, the proposed restrictions can have a positive impact in the quality of the estimates through statistical regularisation. Presently, regularisation methods are a very active area of research in statistical methodology for complex systems (Bickel and Li 2006). The need for regularisation is better understood by discussing the sources of errors in model estimates.

When fitting a model to data, the errors in the estimates can be decomposed into two components: an approximation error and a sample error. The approximation error is the systematic part of the error due to aspects of the data that the model is incapable of capturing. For instance, for the mass-spring-dashpot system shown in Figure 1(i), a model that ignores interactions between the movement of the lumped masses will incur some approximation error whenever the stiffness or damping between the mass elements are non-zero. In such a model, the larger stiffness and/or damping constants of the elements connecting the masses, the larger the approximation error will be. Clearly, models in which more effects are incorporated (larger models) will incur less approximation error.

Sampling errors, the other component of the estimate errors, are due to the random nature of the data. In the presence of random structural loading and measurement errors, no two samples of ambient vibration of a structure will be exactly the same. Such random sources of error cause random fluctuation of the parameter estimates around their expected values. In terms of its sampling error, an estimate is better when the average size of the sampling error is smaller (typically measured by variance and/or standard deviations). A well known fact in the statistics literature is that more complex models tend to be more prone to large sampling errors (see, e.g. Hastie, Tibshirani, and Friedman 2001).

When the number of parameters being adjusted (a proxy for complexity) is small as compared to the sample size, the approximation errors dominate. However, when the number of parameters being estimated is comparable to the sample size, a better estimate may be attained by a smaller model which has a larger approximation error and enjoys smaller sampling error due to noise in the data. In the case at hand, the number of parameters being fit is pq^2. Thus, as the number of sensors increases, the number of parameters being fit rapidly increases and larger sample sizes are needed to fit an adequate model. As a result, restricting the number of parameters being fit can have a beneficial impact on the overall estimation error, especially when the number of sensors on the structure is large.

Of course, not all restrictions to the model are equally desirable. Going back to the example of the ideal mass-spring-dashpot system in Figure 1(i), a model that did not include direct interactions between the lumped masses 1 and 3 would incur no approximation error, but would enjoy a reduced sampling error and thus a smaller total estimation error. This illustrates the fact that not all restrictions are created equal: good restrictions will add little or no approximation error while contributing to reduce sampling error. Thus, the best restrictions are those that reflect

plausible characteristics of the system being modelled. In that spirit, a physical justification of the restricted AR model is presented next.

3.5. *Physical interpretation of the restrictions*

To understand the physical motivation behind the proposed restrictions, consider the simplified mass-spring-dashpot system shown in Figure 1(i) and the corresponding continuous time linear multi degree-of-freedom vibration model (see, for instance, Meirovitch 1986). Let $X_j(t) = [s_j(t) \quad \dot{s}_j(t)]$ denote the state (displacement and velocity) of mass j at time t. From the free body diagram for mass j,

$$\mathrm{d}X_j(t) = \begin{bmatrix} ds(t) \\ \mathrm{d}\dot{s}(t) \end{bmatrix} = \begin{bmatrix} 0 \\ \frac{1}{m_j} \end{bmatrix} f_j(t)\mathrm{d}t - \begin{bmatrix} 0 & 1 \\ k_{jj} & c_{jj} \end{bmatrix} X_j(t) + \sum_{k \in N_i} \begin{bmatrix} 0 & 1 \\ k_{kj} & c_{kj} \end{bmatrix} (X_k(t) - X_j)$$

where k_{kj} and c_{kj} denote the stiffness and damping coefficients of the elements connecting masses k and j.

It follows that, in an infinitesimal time increment $\mathrm{d}t$, the change $\mathrm{d}X(t)$ in the state of mass j is only a function of the state of the masses directly connected to it. In a randomly vibrating system, the state of mass j after an infinitesimal time increment given its current state and that of its direct neighbours is conditionally independent of the state of all other mass elements. In probabilistic terms, that amounts to a Markov property in space (note that the physical model also yields a Markov process in time for the state variables).

If the sampling rate is high *and* the state of the masses is completely observed and the vibrations follows the linear multi degree-of-freedom model, all indirect interactions between non-neighbouring masses could be ignored. That is the motivation behind the proposed restrictions to the multivariate AR model. Due to uncertainties in the model and the state of the system not being directly observable, and the sampling occurring at discrete time steps, an appropriate model for the structure may involve interactions between *higher-order* neighbours. As a result, there is a need for methods for selecting a proper banding parameter w. In Sections 4 and 5, the effects of using different bandwidth parameters are presented.

3.6. *Structural distance versus communication distance*

One important requirement for the applicability of the restrictions proposed here is the agreement of the communication-based distance between nodes and the strength of the physical link between them. The distance defined in Section 3.1 only takes into account the communication cost. Thus a model with lower w will necessarily have a lower communication-cost. However, the physical motivation of the restrictions in Section 3.5 suggests that the spatial restrictions work best when the physical link between nodes that are far apart in the communication topology, $d(i_1, i_2) > w$, is weak.

If strongly connected nodes are far from one another in the communication topology, a larger width w will be needed for the restricted model to fit the data well and as a result the communication benefits of the restriction will be smaller. If all nodes have direct communication links to one another, the restrictions should be adapted to emphasise the strength of the physical connection between the nodes. In this case, the communication topology is not as important an issue as the physical topology defined in terms of direct physical links between elements of the structure.

In the deployment considered in Section 5, the communication and the physical topologies were both linear and the agreement between the distances defined – either in terms of the communication topology of the network or the physical topology of the structure – was perfect.

As long as the communication topology comes close to resembling the physical topology, there is a significant savings in communication by using the restrictions on the AR model to estimate the modal parameter. To illustrate the importance of the interplay between the physical and communication topologies, Figure 1(ii) shows a structure with a more complicated physical topology. Two alternative cases of communication topologies are considered. In the first case, there is a slight mismatch between communication and structural topologies. To account for all the direct physical connections, a $w \geq 3$ must be chosen. For $w = 3$, the second row of $L_j^{(q,w)}$ is

$$\left[L_j^{(w,q)}\right]_{2,\bullet} = \left[\beta_{2,1}^{(w,q)} \quad \beta_{2,2}^{(w,q)} \quad \beta_{2,3}^{(w,q)} \quad \beta_{2,4}^{(w,q)} \quad \beta_{2,5}^{(w,q)} \quad 0 \quad 0 \quad 0\right].$$

In the second case, a larger communication saving is possible since setting $w = 1$ accounts for all the direct structural connections. In this case, the second row of $L_j^{(q,w)}$ with $w = 1$ is

$$\left[L_j^{(w,q)}\right]_{2,\bullet} = \left[\beta_{2,1}^{(w,q)} \quad \beta_{2,2}^{(w,q)} \quad 0 \quad \beta_{2,4}^{(w,q)} \quad 0 \quad 0 \quad 0 \quad 0\right].$$

Note that the matrices of coefficients are no longer banded but are still sparse. Only the correlations between the non-zero entries in the coefficient matrix are needed to estimate them, as was shown in Section 3.2.

Table 1. Modal parameters for the simulated structures.

	Mode	1	2	3	4	5	6	7	8	9	10
Case 1	Frequency (Hz)	3.0	4.4	5.3	7.3	9.1	–	–	–	–	–
	ζ_j (%)	5.0	4.0	3.7	3.6	3.7	–	–	–	–	–
Case 2	Frequency (Hz)	1.6	3.0	4.0	4.7	5.4	6.5	7.6	8.5	9.2	9.6
	ζ_j (%)	5.0	4.0	4.1	4.3	4.6	5.1	5.7	6.2	6.5	6.8

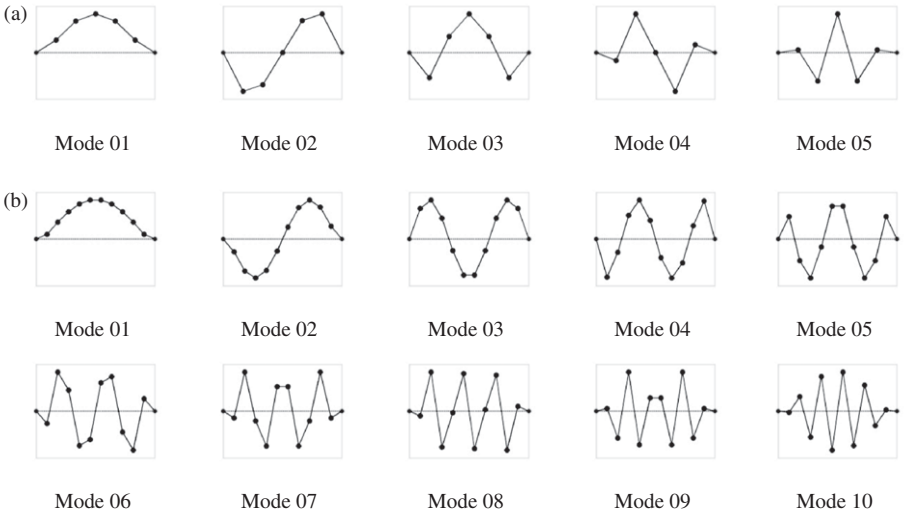

Figure 2. Mode shapes for the simulated structures in (a) Case 1 (five nodes) and (b) Case 2 (10 nodes).

4. Simulated examples

In this section a set of simulated examples is used to compare the performance of modal parameters estimated using the restricted and the full multivariate AR models. Throughout, the AR parameters are estimated using least squares as described in Sections 2.2 and 3.2. The modal parameters are recovered from the estimated AR parameters as described in Section 2.3 for both the restricted and full AR models. Stabilisation diagrams are used to compare the modes identified by each method. The criteria for distinguishing between the computational modes versus the structural modes are described first; then simulation parameters are detailed and the results are presented.

4.1. *Identifying physical modes*

As discussed in Section 2.3, computational modes are removed by discarding modes that are not stable as model order changes. In the stabilisation diagrams shown in Figures 3, 4 and 6, only the 'locally stable' modes are shown. A mode from the (full or restricted) $AR(q)$ model is considered 'locally stable' if its variation from the $AR(q-2)$ model for frequency, damping ratio and mode shape colinearity are below 2%, 5% and 5%, respectively (Pappa, Elliott, and Schenck 1993; De Roeck, Claesen, and Van Den Broeck 1995). While the stabilisation diagram for the two methods may appear different, the important feature for comparison is whether the same modes appear as 'locally stable' for different number of $AR(q)$ models. In short, the stabilisation diagrams show whether structural modal properties are consistently identified using models with varying number of lags.

4.2. *Simulation set-up*

Two structures with linear topology and lumped masses are used for simulation. Figure 1(ia) shows the schematic of one of the structures with five lumped masses and linear stiffness and damping components connecting them. The second simulated case has a similar structure, but with 10 lumped masses instead of five. In each case the acceleration response of the structure to white noise excitation is simulated at each mass and the performance of the restricted and full

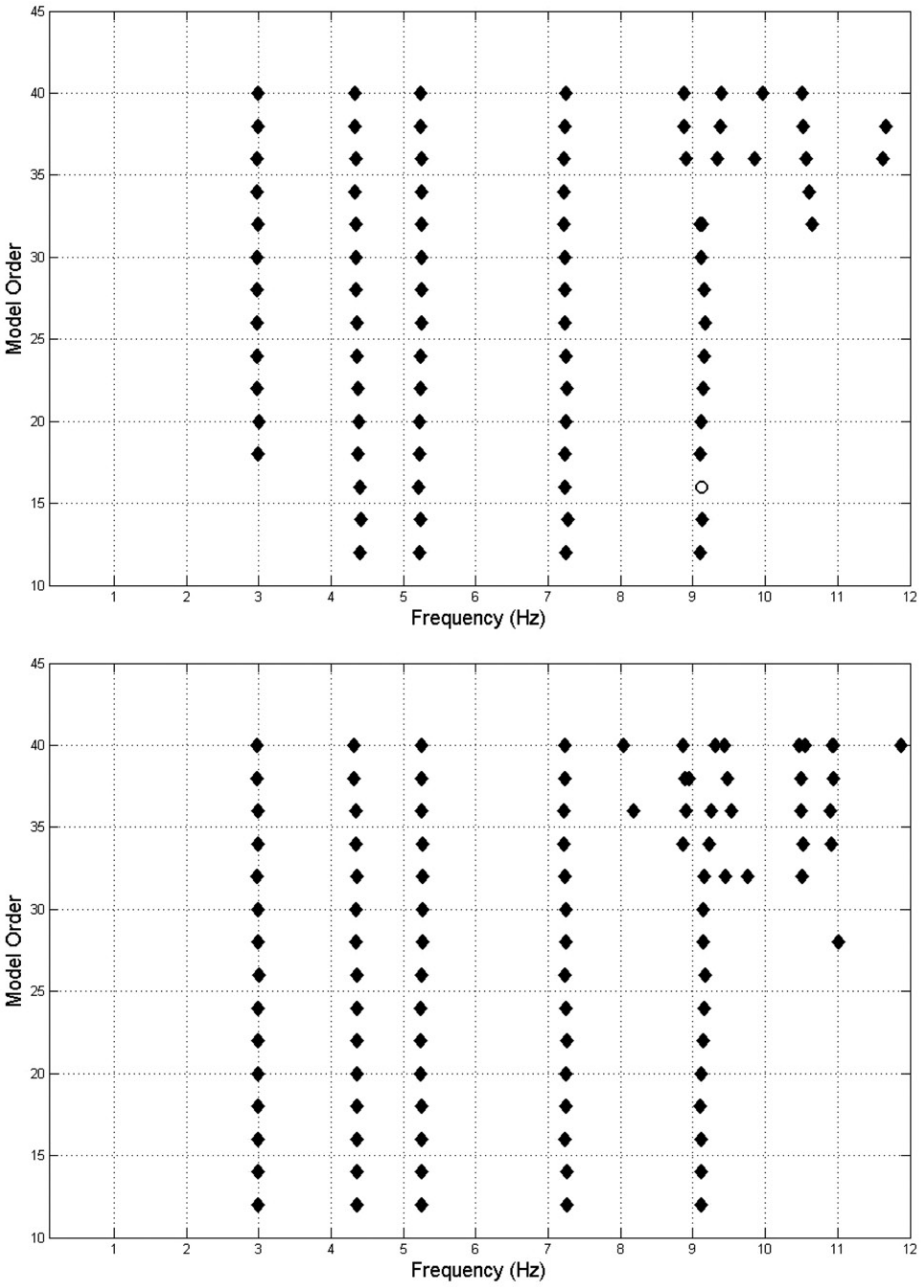

Figure 3. Stabilisation diagrams for the five-DOF simulated system for the restricted model with $w = 1$ (a) and unrestricted model (b).

$AR(q)$ models are compared for different neighbourhood width w for the restricted coefficient matrices. Stabilisation graphs, with the lags ranging from 5 to 40 are used to show the rate of convergence of the results (Pakzad and Fenves 2009). Cases 1 and 2 correspond, respectively, to the five and ten degree of freedom structures whose modal parameters are listed in Table 1 and mode shapes as shown in Figure 2. The performances of the full and restricted AR models in identifying modes are compared through their stabilisation diagrams.

4.3. *Results for case 1: five degrees of freedom system*

Figure 3 shows a comparison between the stabilisation diagrams obtained using the restricted AR model with

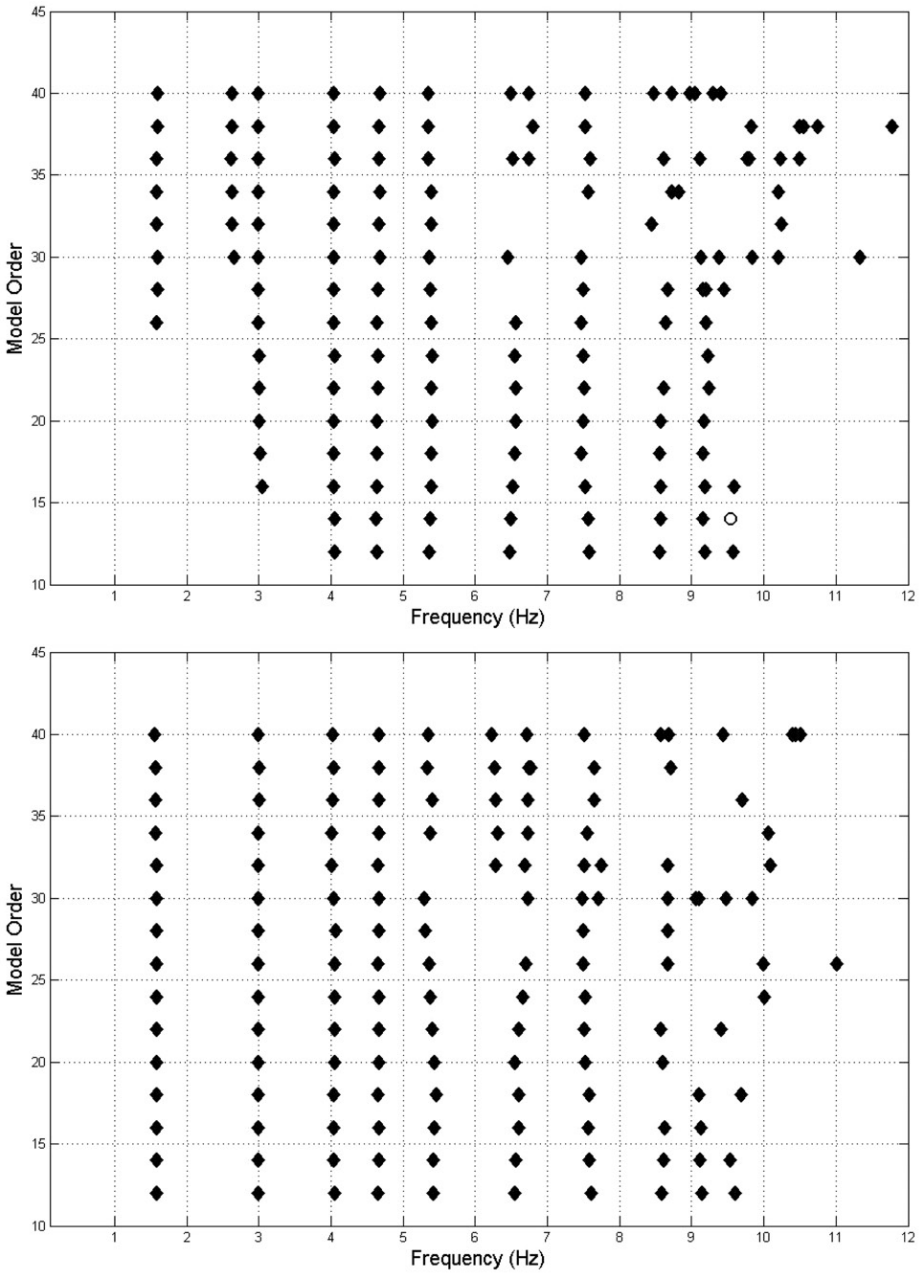

Figure 4. Stabilisation diagrams for the 10-DOF simulated system for the restricted model with $w = 2$ (a) and unrestricted model (b).

$w = 1$ and the full AR model. It must also be noted that the stabilisation diagrams can only be used in conjunction with engineering knowledge from the structure. In this case, for example, there is considerable noise in both restricted and full models for the frequencies above 9.1 Hz which is due to over-parameterisation of each model for higher model orders. In each case, however, a lower model order is sufficient for modal identification and the analysis can stop when lag order is 18. For both the restricted and the full AR model the number of lags varies from 5 to 40. The stabilisation graph for the restricted AR model shows the five estimated modes converging with a small number of lags while its communication load is only 53% of the full model. The stabilisation graph for the full model is practically identical to the case with $w = 2$ (not shown) in that the same five stable modes are identified. In that case, the communication load,

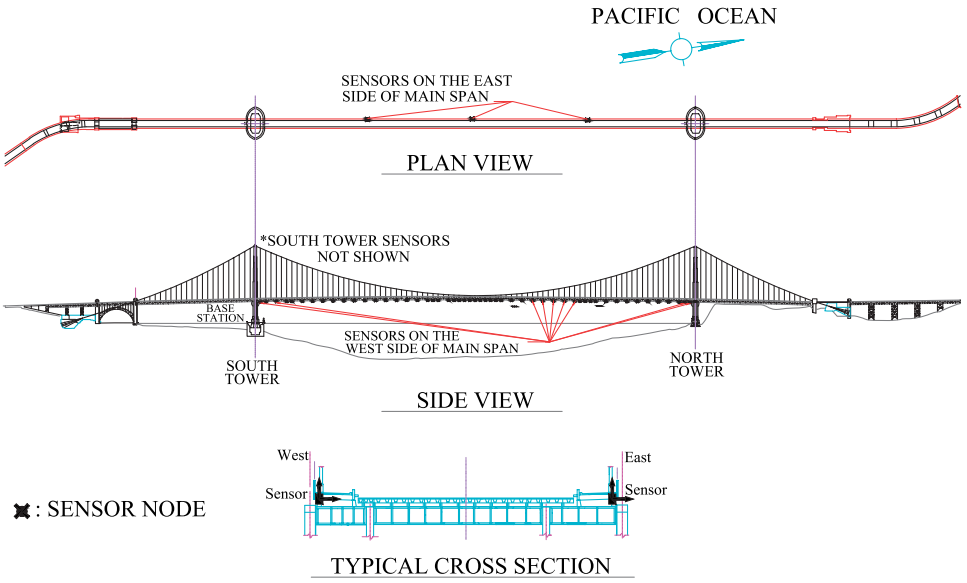

Figure 5. Plan and elevation views of GGB and the location of the wireless sensors on the main-span.

as measured by the number of transmitted data packets, is 93% of the full model. Interestingly, the stabilisation diagrams for $w = 0$ (not shown) suggest that even when cross-correlation coefficients are completely disregarded, the natural frequencies were correctly identified.

4.4. *Results for case 2: ten degrees of freedom system*

Figure 4 shows similar stabilisation diagrams for the 10-DOF case. Here, the comparison is between the restricted AR model with $w = 2$ and the full AR model. Using only 62% of the number of transmitted data packets of the full AR model, the restricted model managed to consistently identify all modes below 8 Hz. For the modes above 8 Hz, both methods had trouble in consistently identifying modes.

5. Testbed on GGB

Figure 5 shows GGB at the entrance of the San Francisco Bay, which has a 1280 m (4200 ft) long main-span and 343 m (1125 ft) side-spans. Two stiffening trusses support an orthotropic roadway deck and horizontal planes of wind bracing system at the bottom plane of the truss chords. The legs of the towers, 210 m (745 ft) above the water level, have cellular box sections, connected by horizontal struts at seven elevations (Strauss 1937; Stahl, Mohn, and Currie 2007). The WSN that collected the data used in this article was deployed on the bridge to measure and record ambient accelerations. The sensor network consisted of 64 nodes on the main-span and the south tower of the bridge. The network was designed to be scalable in terms of the number of the nodes, complexity of the network topology, data quality and quantity by addressing integrated hardware and software systems such as sensitivity and range of (MEMS) sensors, communication bandwidth of the low-power radio, reliability of command dissemination and data transfer, management of large volume of data and high-frequency sampling (Pakzad et al. 2008). The nodes on the main-span measure acceleration in vertical and transverse directions (Pakzad and Fenves 2009). On the tower, the nodes measure acceleration in transverse and longitudinal directions.

The instrumentation plan for the WSN for the bridge is also shown in Figure 5. The nodes on the main-span were located based on the range of the radio transmission distance at 30.5 m (100 ft) spacing, but a 15.25 m (50 ft) spacing was used where an obstruction hindered radio communication. Each main-span node was attached to the top flange of the floor girder directly inside of the cable. The eight nodes on the south tower were placed at the ends of four struts above the roadway. The tower nodes have a clear line of sight between them and hence have greater radio range than the main-span nodes. The node on the west side of the strut above the superstructure collects data from all the nodes on the tower and transmits them to the network on the main-span. Fifty-three nodes were installed beginning on 10 July 2006, on the west side of the main-span. On 15 September 2006, batteries were replaced for the nodes on the main-span and three extra nodes were added on the east side. The east side

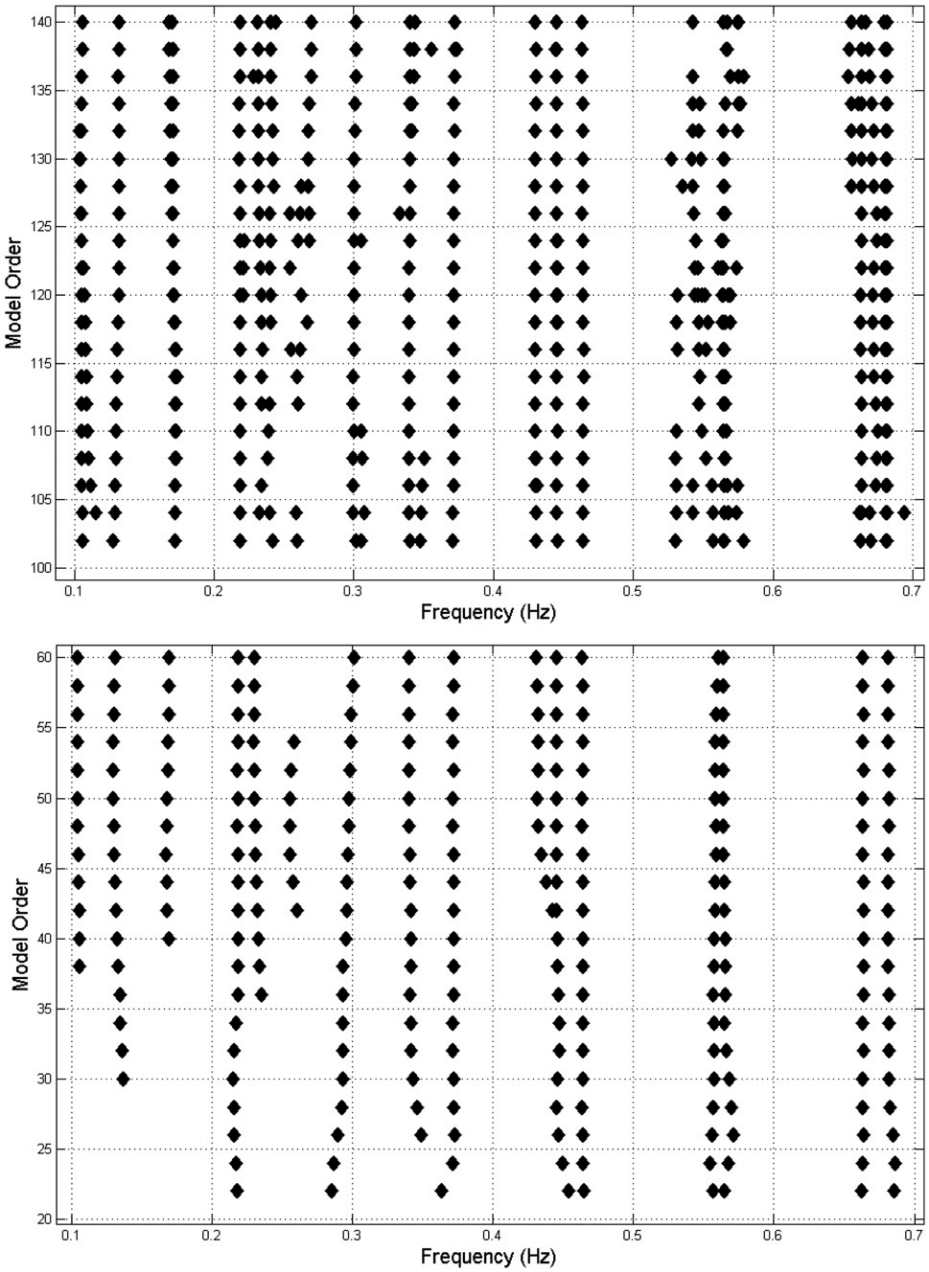

Figure 6. Stabilisation graph for vertical and torsional modes for the restricted model with $w = 8$ (a) and unrestricted model (b).

nodes were located at the two quarter-spans and the mid-span of the bridge and had radio communication with the west side nodes under the roadway deck. There were a total of 174 data collection runs of the network during the deployment which lasted until 14 October 2006, including testing and debugging, so not all of the collected data sets contain data from all of the nodes.

The sampling rate for all runs was 1 kHz, but since the significant vibration frequencies of the bridge are much lower, the data were averaged on the node and downsampled to 50 to 200 Hz prior to transmission. In some of the runs all five channels on a node (two high-level motion sensors, two low-level motion sensors and the temperature sensor) were sampled, but in other runs the channels were limited to the low-level accelerometers to reduce the volume of data. The 512 kB flash memory of each node can buffer 250,000 samples of data, which may be allocated to any combination of the five sensor channels on the node

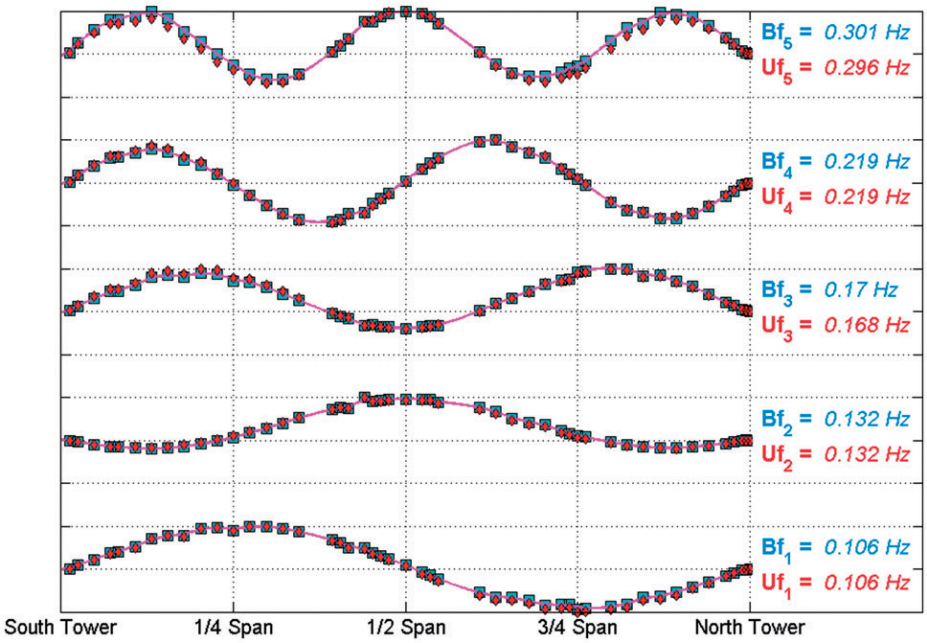

Figure 7. Comparison of the identified vertical modes 1 through 5, using restricted model (in blue) versus unrestricted model (in red).

(four accelerometer channels and a temperature sensor). Each run started with a pause to synchronise the network and disseminate a command to start sampling at a future time. After the scheduled sampling took place, there was a pause to establish the network routing. The recorded data were then transferred from each node to the base station using reliable data communication and pipelining. Each run generated up to 500 kB data per node, which for the network of 60 nodes produced 30 MB data for 15 million samples. Approximately 1.3 GB data was collected during the deployment of the WSN on GGB.

5.1. *Modal identification of GGB*

In this section the modal properties of the main-span of the bridge are presented. The results are obtained by using least squares to estimate the parameters of the full and restricted AR with different diagonal bandwidth w. The modal parameters using different values of w are estimated and compared. For the restricted model, the bandwidth parameter was set at $w = 8$. Reducing the bandwidth further caused sensible changes in the stabilisation plots whereas increasing w did not. Figure 6 shows the stabilisation diagrams for the two cases. The presented results are limited to 0.7 Hz in order to avoid cluttering of the graphs. Note that although the number of lags used by the restricted model is higher than in the unrestricted case, the results show an excellent match. The identified vertical and torsional modes for each case are presented in Figures 7–9. The presented results are limited to approximately 0.7 Hz again, to avoid repetitive plots. The only significant discrepancy between the two models is in the second torsional mode, where the restricted model identifies a mode at frequency 0.24 Hz, while the unrestricted model misses this mode completely. This mode with no node is consistent with the expected dynamic behaviour of the bridge as a system with distributed mass and elasticity which has a purely translational mode. The previous study of the bridge by Abdel-Ghaffar and Scanlan (1985a) also confirms the validity of this torsional mode. Some minor discrepancies are observed in the 0.5 Hz–0.7 Hz, which can be attributed to the larger number of lags used by the restricted model resulting in a larger number of computational modes around the physical modes. In terms of the volume of communication, Equation (9) shows that the volume of transmitted data needed to fit the restricted AR would be 29% of the volume required by the full AR model.

6. Conclusion

Multivariate AR models are commonly used to model the dynamic behaviour of vibrating structures and to infer the modal parameters of a structure that is subjected to ambient vibration. In this article,

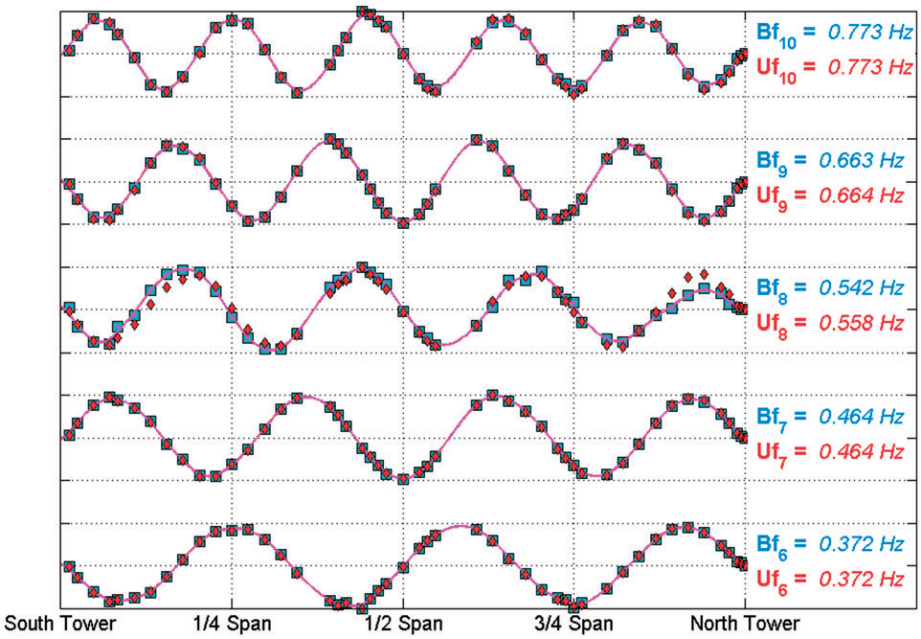

Figure 8. Comparison of the identified vertical modes 6 through 10, using restricted model (in blue) versus unrestricted model (in red).

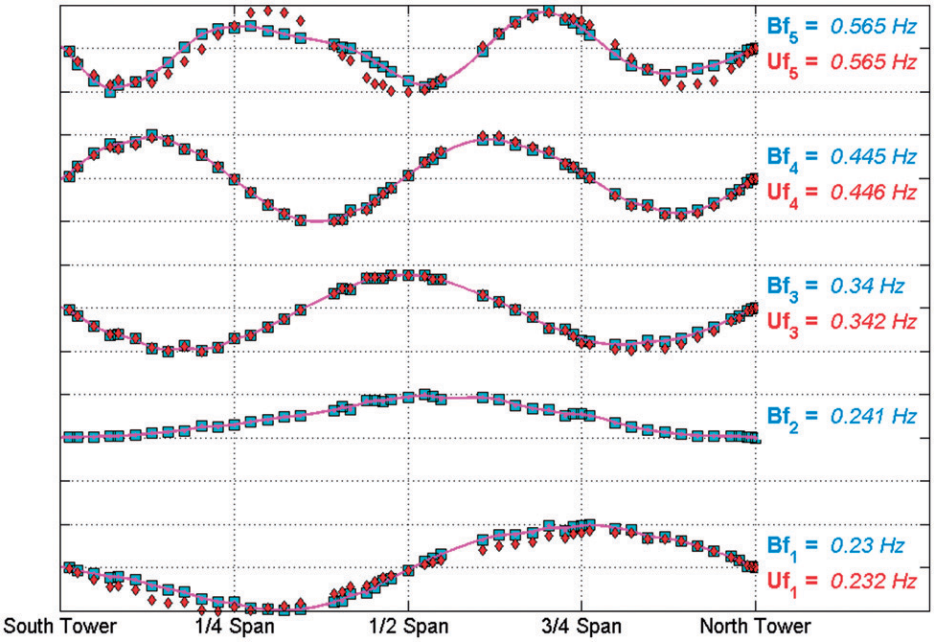

Figure 9. Comparison of the identified torsional modes 1 through 5, using restricted model (in blue) versus unrestricted model (in red). The second mode shape corresponds to a mode only identified by the restricted AR model.

a restricted version of the multivariate AR model is presented that can significantly reduce the volume of transmitted data over a WSN while introducing little distortion on the modal parameter estimates. A physical motivation for the set of proposed restrictions is given.

Simulated data of structures with linear topology are used to show that the restricted models can recover the modal parameters while reducing the volume of transmitted data. Comparison of the application of the restricted and full AR models to data collected by a WSN deployed on the GGB shows that, with a properly chosen bandwidth, the modal parameter estimates are comparable in both cases. In addition, the restricted model is able to

identify an additional torsional mode for the structure.

Future work will be devoted to proposing a methodology for selecting an appropriate set of restrictions to the AR models and the analysis of the savings that can be achieved in structures with alternative topologies.

Acknowledgements

This work reflects the advice and guidance of Professors Gregory Fenves, David Culler, and James Demmel. Dr Sukun Kim developed the software and closely collaborated in design of hardware and deployment of the network on GGB. The authors give special thanks to the staff and management of GGB, Highway and Transportation District, in particular Dennis Mulligan and Jerry Kao, for their close cooperation in every step of the project. Jorge Lee provided extraordinary help in the deployment, which made this project possible. This research was partially supported by the National Science Foundation under grant Nos. EIA-0122599, 0926898, NSF DMS-0907632, and SES-0835531 (CDI).

Notes on contributors

Shamim Pakzad is P.C. Rossin Assistant Professor in Civil and Environmental Engineering department at Lehigh University. He received his BS in civil engineering from BIHE in Iran (1995), MS from San Jose State University (2000) and PhD from University of California, Berkeley (2008), both in civil and environmental engineering, with minors in statistics and signal processing. He is a member of several professional organisations including American Society of Civil Engineers (ASCE), Structural Engineering Institute (SEI) and the Consortium of Universities for Research in Earthquake Engineering (CUREE). His research interests are in the application of WSNs in structural engineering, structural dynamics, health monitoring of bridges and statistical damage detection methods.

Guilherme Rocha received his BA in Mechanical Engineering from the University of Sao Paulo in 1999, his MS in Economics from the Getulio Vargas Foundation in 2003 and a PhD in Statistics from University of California, Berkeley in 2008. He is interested in applications of Statistics to massive high dimensional data sets.

Bin Yu is Chancellor's Professor in the departments of Statistics and of Electrical Engineering and Computer Science at UC Berkeley. She is currently the chair of department of Statistics, and a founding co-director of the Microsoft Lab on Statistics and Information Technology at Peking University, China. She got her BS in mathematics from Peking University in 1984, MS and PhD in Statistics from UC Berkeley in 1987 and 1990. She has published over 80 papers on a wide range of research areas including empirical process theory, information theory (MDL), MCMC methods, signal processing, machine learning, high dimensional data inference (boosting and Lasso and sparse modelling in general), bioinformatics and remotes sensing. She has been and is serving on many leading journals' editorial boards including *Journal of Machine Learning Research*, *The Annals of Statistics* and *Technometrics*. Her current research interests include statistical machine learning for high dimensional data and solving data problems from remote sensing, neuroscience and newspaper documents. She was a 2006 Guggenheim Fellow, and is a Fellow of AAAS, IEEE, IMS (Institute of Mathematical Statistics) and ASA (American Statistical Association).

References

Abdel-Ghaffar, A.M., and Scanlan, R.H. (1985a), 'Ambient Vibration Studies of Golden Gate Bridge: I Suspended Structure', *Journal of Engineering Mechanics (ASCE)*, 111, 463–482.

Abdel-Ghaffar, A.M., and Scanlan, R.H. (1985b), 'Ambient Vibration Studies of Golden Gate Bridge: II Pier-tower Structure', *Journal of Engineering Mechanics (ASCE)*, 111, 483–499.

Andersen, P. (1997). 'Identification of Civil Engineering Structures Using Vector ARMA Models', PhD dissertation, Aalborg University, Department of Building Technology and Structural Engineering, Denmark.

Bickel, P.J., and Li, B. (2006), 'Regularization in Statistics', *Test*, 15, 271–344.

Chang, C.C., Chang, T.Y.P., and Zhang, Q.W. (2001), 'Ambient Vibration of Long-span Cable-stayed Bridge', *Journal of Bridge Engineering (ASCE)*, 6, 46–53.

Cunha, A., Caetano, E., and Delgado, R. (2001), 'Dynamic Tests on Large Cable-stayed Bridge', *Journal of Bridge Engineering (ASCE)*, 6, 54–62.

De Roeck, G., Claesen, W., and Van Den Broeck, P. (1995), 'DDS-methodology Applied to Parameter Identification of Civil Engineering Structures', in *Proceedings of Vibration and Noise '95*, Venice, Italy, pp. 341–353.

Doebling, S.W., Farrar, C.R., and Prime, M.B. (1998), 'A Summery Review of Vibration-based Damage Identification Methods', *The Shock and Vibration Digest*, 30, 91–105.

Farrar, C.R. (2001), *Historical Overview of Structural Health Monitoring*, Lecture Notes on Structural Health Monitoring using Statistical Pattern Recognition, Los Alamos, NM: Los Alamos Dynamics.

Glaser, S.D., and Tolman, A. (2008), 'Sense of Sensing: From Data to Informed Decisions for the Built Environment', *Journal of Infrastructure Engineering (ASCE)*, 14, 4–14.

Hastie, T., Tibshirani, R., and Friedman, J. (2001), *The Elements of Statistical Learning: Data Mining, Inference and Prediction*, New York: Springer.

Kim, S., Pakzad, S.N., Culler, D., Demmel, J.,Fenves, G.L., Glaser, S. and Turon, M. (2007), 'Health Monitoring of Civil Infrastructures Using Wireless Sensor Networks', in *Proceedings of the 6th International Conference on Information Processing in Sensor Networks (IPSN 2007)*, Cambridge, MA.

Lembregts, F., Snoeys, R., and Leuridan, J. (1992), 'Application and Evaluation Multiple Input Modal-parameter Estimation', in *Proceedings of the 17th International Seminar on Modal Analysis – Course on Modal Analysis Theory and Practice*, Leuven, Belgium.

Meirovitch, L. (1986), *Elements of Vibration Analysis*, New York: McGraw-Hill.

Olfati-Saber, R. (2007), 'Distributed Kalman Filtering for Sensor Networks', in *Proceedings of 46th IEEE Conference on Decision and Control*, New Orleans, LA.

Pakzad, S.N. (2010), 'Development and Deployment of Large Scale Wireless Sensor Network on a Long-span Bridge', *Smart Structures and Systems, An International Journal*, 6, 525–543.

Pakzad, S.N., and Fenves, G.L. (2009), 'Statistical Analysis of Vibration Modes of a Suspension Bridge Using Spatially Dense Wireless Sensor Network', *Journal of Structural Engineering (ASCE)*, 135, 863–872.

Pakzad, S.N., Fenves, G.L., Kim, S., and Culler, D.E. (2008), 'Design and Implementation of Scalable Wireless Sensor Network for Structural Monitoring', *Journal of Infrastructure Engineering (ASCE)*, 14, 89–101.

Pandit, S.M. (1991), *Modal and Spectrum Analysis: Data Dependent Systems in State Space*, New York: John Wiley and Sons.

Pappa, R.S., Elliott, K.B., and Schenck, A. (1993), 'Consistent Mode Indicator for Eigen System Realization Algorithm', *Journal of Guidance, Control and Dynamics*, 16, 852–858.

Peeters, B., and Roeck, G.D. (2001), 'Stochastic System Identification for Operational Modal Analysis: A Review', *Journal of Dynamic Systems, Measurement, and Control*, 123, 659–667.

Shen, B., Wang, Z., and Hung, Y.S. (2010), 'Distributed Consensus H-infinity Filtering in Sensor Networks with Multiple Missing Measurements: The Finite-horizon Case', *Automatica*, 46, 1682–1688.

Sohn, H., Farrar, C.R., Hemez, F.M., Czarnecki, J.J., Shunk, D.D., and Stinemates, D.W. (2004), 'A Review of Structural Health Monitoring Literature: 1996–2001', Report No.: LA-13976-MS, Los Alamos National Laboratory, Los Alamos, LM.

Stahl, F.L., Mohn, D.E., and Currie, M.C. (2007), 'The Golden Gate Bridge,' Report of the Chief Engineer (Vol. II), San Francisco, CA: Golden Gate Bridge and Transportation District.

Strauss, J.B. (1937). 'The Golden Gate Bridge', Report to the Board of Directors of the Golden Gate Bridge and Highway District, California, September 1937.